

Application of Near IR, Phase-Contrast Imaging to Backside Failure Isolation and Analysis

R. Aaron Falk

OptoMetrix, Inc., Renton, Washington

Edward W. Budiarto

Intel Corporation, Hillsboro, Oregon

Abstract

The move towards flip-chip type packaging has produced significant obstacles for failure analysis. One such obstacle is the breakdown of traditional techniques for failure isolation via thermal mapping, typically used to isolate short circuits and leakage paths. This paper describes the application of near infrared (IR) phase-contrast techniques to allow highly sensitive, ~ 10 mK, thermal mapping for backside failure analysis.

Introduction

The traditional topside thermal mapping techniques of liquid crystal imaging and fluorescent micro-thermal imaging (FMI) are considerably less effective from the backside due to the heat diffusion caused by the intervening silicon substrate. The presence of the substrate can be taken to advantage, however, by detecting the localized changes in its optical properties brought about by a heat source.

Silicon has a refractive index change of $\sim 5 \times 10^{-5}$ per $^{\circ}\text{C}$. GaAs has a coefficient of $\sim 3 \times 10^{-4}$ per $^{\circ}\text{C}$. Although small, these changes can be imaged using laser-probing techniques and phase imaging. In particular, the form of phase imaging known as Schlieren imaging offers extraordinary sensitivity using standard laser and high-resolution CCD camera components.

Refractive Index Effects in Semiconductors

The refractive index of semiconductor materials depends on a number of parameters with temperature being one of the dominant effects. For backside analysis tools, the primary interest is in wavelengths with energies below the semiconductor bandedge. These wavelengths can pass through the substrate with minimal absorption [1]

Experimental data for the refractive index of GaAs versus temperature for photon energies at or below

the gap energy is available from the work of D.T.F. Marple [2]. As seen in the graph of the data in their Figure 15, the shift in refractive index versus temperature shrinks slightly with wavelength over the region of 0.85 to 1.7 micron. At 1.06 micron, where GaAs is fairly transparent the shift in refractive index between 300K and 187K is approximately 2.6×10^{-4} (1/K) and between 187K and 103K is 2.4×10^{-4} (1/K), which are equal within the error of the data extraction process. The average of the two is adopted

$$\frac{\partial n_{\text{GaAs}}}{\partial T} \cong 2.5 \times 10^{-4} \text{ (1/K)} \quad (1)$$

No experimental data for the change in refractive index with temperature for silicon could be found in the literature. An alternative method for determining a value utilizes the shift in bandedge with temperature combined with the shift in refractive index with photon energy. An empirical formula due to Y.P. Varshni [3] for the bandedge shift is

$$\Delta E_g = \frac{aT^2}{T + b}, \quad (2)$$

with values of $a=7.021 \times 10^{-4}$ (eV/K) and $b = 1108$ K being the currently accepted values for silicon. If the refractive index of the semiconductor is known as a function of photon energy (wavelength), then, to a first approximation

$$\frac{\partial n}{\partial T} \cong \frac{\partial n}{\partial E_{ph}} \frac{\partial E_g}{\partial T}. \quad (3)$$

The refractive index values at photon energies of 0.809, 0.885, and 1.033 eV [4] were used to obtain the shift in refractive index versus photon energy yielding

$$\frac{\mathcal{I}n_{Si}}{\mathcal{I}E_{ph}} \cong 0.17 (1/eV), \quad (4)$$

which in combination with Equation (3) yields

$$\frac{\mathcal{I}n_{Si}}{\mathcal{I}T} \cong 4.6 \times 10^{-5} (1/K). \quad (5)$$

This same approach can be used to estimate absorption shifts and was verified against measured values of the relative absorption of silicon by K. Bucher et al. [5].

Schlieren Imaging

Classical Schlieren imaging, as shown in Figure 1, utilizes a knife-edge to partially block the optical beam on its way to the image plane [6]. In the upper illustration in Fig. 1, Lens 1 focuses a beam of rays from the source onto a transparent object. Lens 2 re-collimates the beam, which is then re-focused onto the image plane by Lens 3. A knife-edge is placed in the focal plane of Lens 2, where an image of the

source is formed, such that it partially blocks the source image. The lower illustration in Figure 1 is identical to the upper, except that the object causes the rays passing through it to be deviated by a small angle α . This angular deviation in the object plane results in a positional shift of the source image at the knife-edge. The intensity in the image plane of the

Schlieren arrangement is thus proportional to the angular deviation caused by the object.

Angular deviations can be caused by geometric variations in the object. The first historical use of a Schlieren imaging system was the Foucault knife-edge test, which allowed observation of minute geometrical errors in the surface of optical components. A non-uniform refractive index also causes angular deviations of magnitude proportional to the spatial derivative of the refractive index. The angular sensitivity of a Schlieren system is measured in micro-radians, which translates to refractive index deviations on the order of 10^{-6} .

Figure 1 illustrates a transmission mode Schlieren arrangement. A reflection mode arrangement, which is needed to examine an IC, is obtained by folding the transmission system about the object plane (Lens 1 and Lens 2 merge) and adding a beam splitter. The sensitivity of a Schlieren system is proportional to the source intensity, while being inversely proportional to the source size. This combination requires a high source irradiance, which suggests the high intrinsic brightness of a laser source. In addition, the source wavelength must be matched to the transmission characteristics of the test material. This requirement suggests a wavelength around 1060 nanometers for silicon [1]. A high-resolution imaging detector is also needed with a computer interface for image acquisition and processing. Digital CCD cameras offer reasonable sensitivity at the required wavelength with high-resolution imaging formats of 1024x1024 and 2048x2048 pixels coupled with 10 and 12 bit intensity resolution.

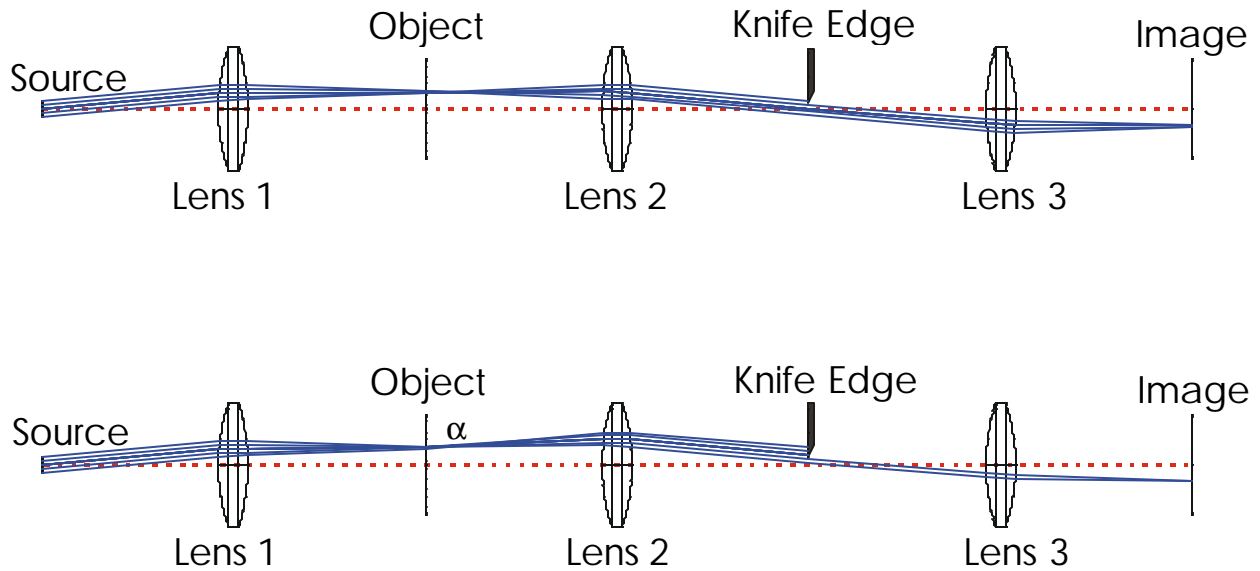


Figure 1 Ray traces of Schlieren imaging arrangement using ZEMAX® optical analysis software. Upper and lower traces indicate effect of deviation of the optical beam by the object.

A useful Schlieren imaging system does not simply consist of the optics. Figure 2 is a schematic overview of a complete system, including digital frame grabbing, timing circuitry for controlling the state of the device in coincidence with the image acquisition, staging and navigation, and overall computer control of the data acquisition and processing.

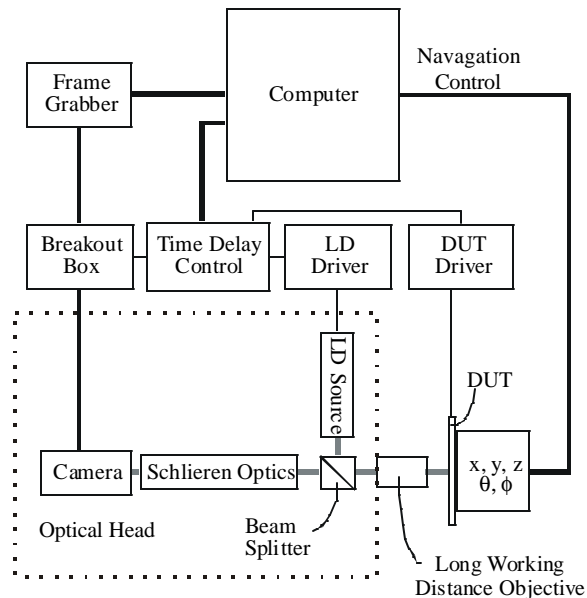


Figure 2 Schematic overview of complete Schlieren imaging system.

Some example imagery is shown in Figures 3 and 4. Figure 3 shows a standard reflection image of a metal film target. The dark areas are the places where the metal film was removed. The Schlieren filter in the image in Figure 4 was set to block all the light from the flat portions of the target. This background is suppressed, leaving only light that was deflected from the film edges.



Figure 3 Reflected light image of metal film resolution target.

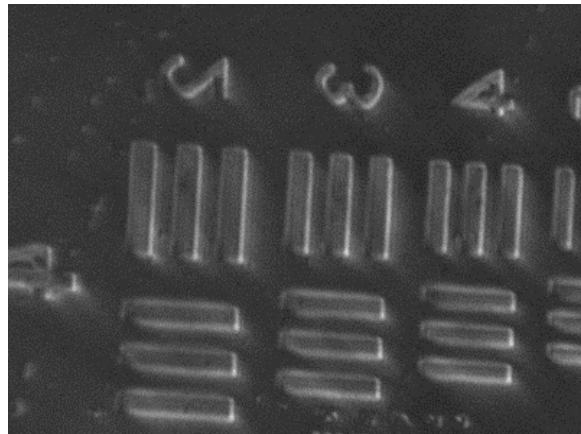


Figure 4 Schlieren image of same target. Slopes at metal edges, which deviate the optical beam are enhanced while the flat background is suppressed.

Scaling

A significant advantage of the Schlieren approach to phase contrast imaging is how it scales with the size of the target. For small changes in the refractive index, the angular deviation of the optical path within the substrate is given by [6]

$$\mathbf{e}_{\text{int}} \cong \int \frac{1}{n} \frac{\nabla n}{\nabla x} dz \cong \frac{1}{n_0} \int \frac{\nabla(\Delta n)}{\nabla x} dz \quad (6)$$

where z is the optical axis, x is a transverse direction, and n is assumed to be the sum of the substrate refractive index, n_0 , and a small perturbation, Δn . The external angular deviation relates to the internal deviation via Snell's law, which for small angles near normal incidence, yields

$$\mathbf{e}_{\text{ext}} \cong \int \frac{\nabla(\Delta n)}{\nabla x} dz \quad (7)$$

As a target is scaled down, the x and z components will scale proportionately, which leaves the angular deviation constant.

As an example, a cylindrically symmetric target with a radial distribution given by

$$\Delta n = \Delta n_0 \exp(-r^2/a^2) \quad (8)$$

is assumed where Δn is the refractive index change in the target, with Δn_0 being the peak value, r is the radial distance and a is the effective radius of the filament.

Utilization of the distribution model in Eq. 8 yields

$$\mathbf{e}_{ext} \cong -\frac{2\sqrt{p}\Delta n_0 x}{a} \exp(-x^2/a^2) \quad (9)$$

with a peak deviation given by

$$\mathbf{e}_{peak} \cong -\sqrt{2p}\Delta n_0 \exp(-1/2) = -1.5\Delta n_0 \quad (10)$$

The peak deviation, which sets the sensitivity limit, is independent of the radius, a . Other phase contrast techniques, e.g. interferometry, have sensitivity that falls off at least linearly with the scale size. The independence of Schlieren imaging with scale size represents a significant advantage as device size decreases.

Results

Our initial experimental efforts utilized a transmission mode instrument to image transient breakdown effects in a GaAs switch [7]. The switch

was biased at several kilovolts and transitioned to a low conduction state when illuminated with a fast optical pulse. Lifetime was a significant issue with the switch. Schlieren images of the switch, shown in Figure 5, demonstrated the existence of filaments with a rapidly rising temperature. The actual temperature was extracted by fitting the data to a Gaussian temperature profile as shown in Figure 6. For the images shown, the temperature rose ~ 12 K in less than 40 nanoseconds.

Although the GaAs switch operated at high-voltages and high-currents, it was also rather large. The electric fields, carrier densities, and temperatures of the switch were very similar to those found in standard semiconductor devices. This reasoning initiated the development of a second, reflection mode, Schlieren instrument for measuring temperature variations in silicon semiconductors. Figure 7 shows a photo of this prototype instrument. This instrument demonstrated the capability of reflected light and Schlieren thermal imagery from the backside of flip-chip type integrated circuits as shown in Figures 8 and 9.

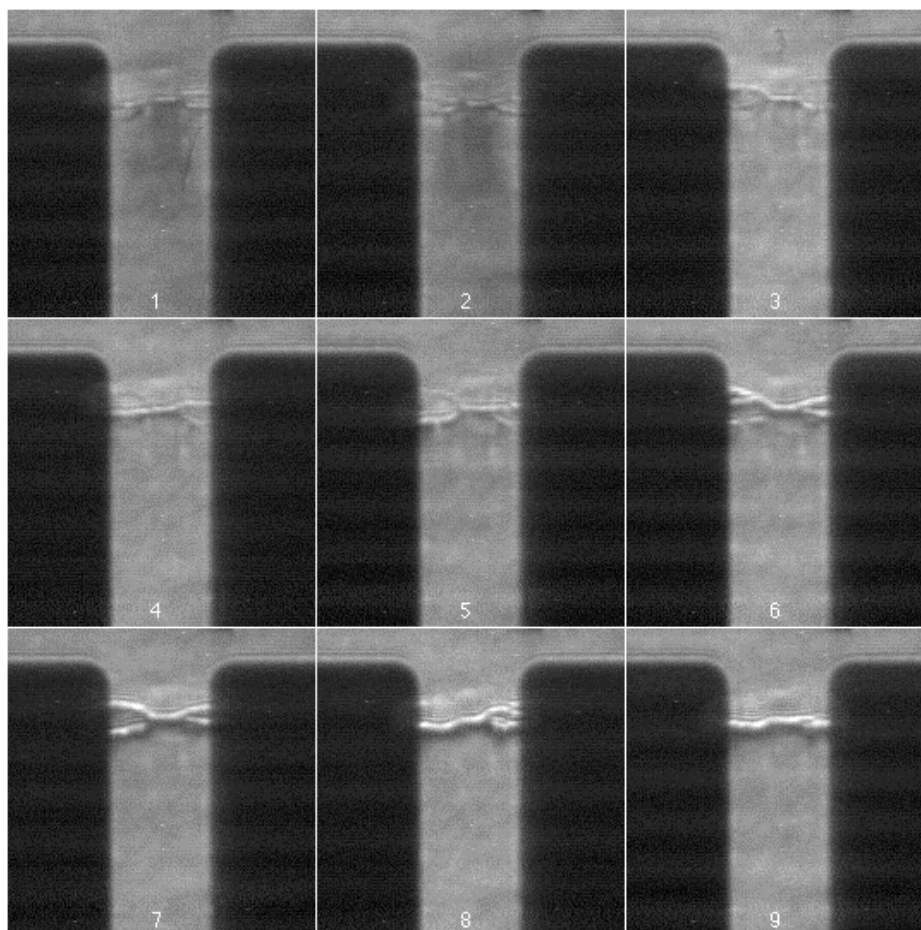


Figure 5 Montage of 9 images with 5 nanosecond delay between each image. Evolution of filaments to higher temperatures is apparent. Electrode spacing is 1 millimeter.

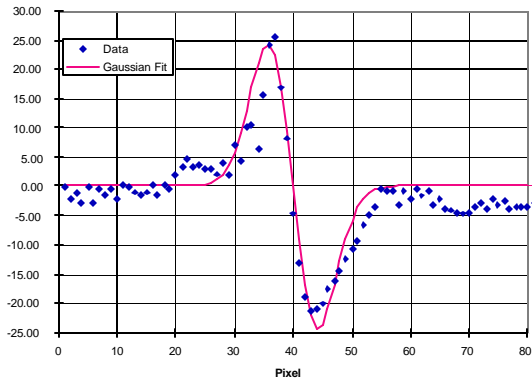


Figure 6 Fit a vertical slice of filament intensity minus background to the expected intensity for cylindrical Gaussian refractive index profile.

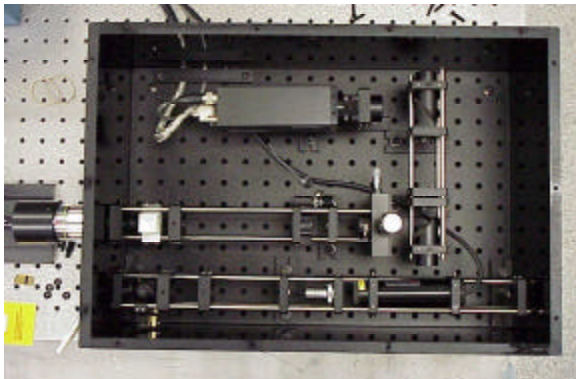


Figure 7 Photo of early prototype Schlieren Thermal Mapper (STM).

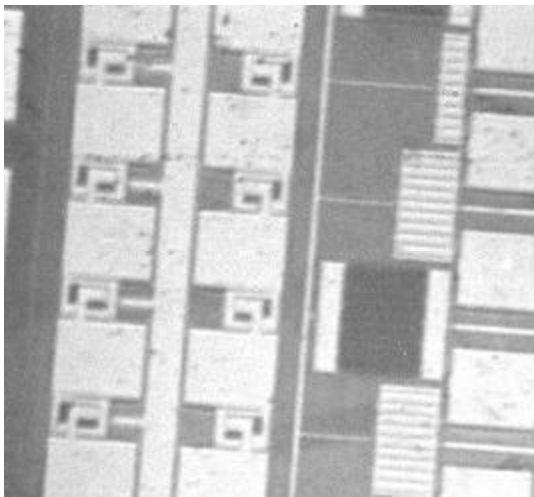


Figure 8 Backside reflected light image obtained using STM.

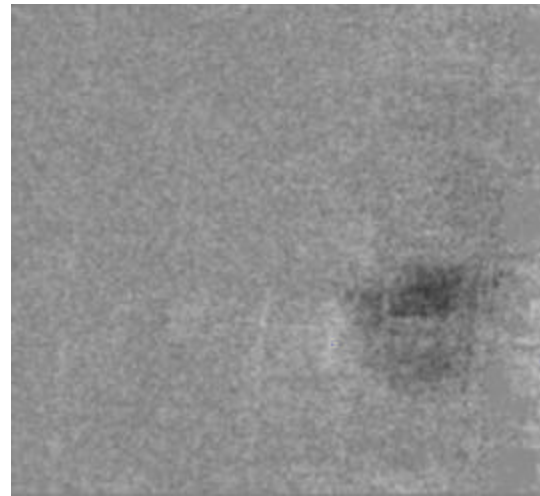


Figure 9 Real-time Schlieren thermal image of area shown in Figure 8. Temperature rise is estimated at ~ 1 K.

The test structure in Figures 8 and 9 consists of a series of metal lines ($0.8 \times \sim 90$ microns) separated by 12 microns. The metal is a stack of Ti, Ti-nitride, and Al-Cu alloys, though, for all practical purposes, it can be considered as just aluminum. The lines are at the metal 1 (M1) layer, the first metal layer above the Si-substrate and SiO₂ layer. The lines are closely surrounded/enclosed by a 100×120 -micron metal structure at the same M1 layer, so that the heat source is, for practical purposes, that same size. Adjacent metal lines are then connected to each other, to form a serpentine structure, by contact vias and metal pads at the metal 2 (M2) layer. There is an oxide layer between M1 and M2 layers. This structure is an EM (Electro-Migration) structure normally used to study the electro-migration properties of the metal stack.

The backside of the sample was ground back to ~ 200 micron thickness, was polished to an optical finish and an AR (anti-reflection) coating applied. The sample was then mounted into a standard package with a portion of the package bottom removed for optical access to the backside of the sample.

To calibrate the temperature, the structure is put in an oven with a controlled temperature. At equilibrium, the structure's temperature is assumed to be the same as the oven's. A low current is passed through the structure to measure its resistance. The current is low enough that self-heating is negligible. The resistance versus temperature can be found in this manner. Once we know R vs. T , we can use the structure as its own thermometer.

The limiting sensitivity of this early prototype system was ~ 50 mK, 5 to 12 times better than data taken with a passive infrared thermal imaging system. The

results are comparable to FMI measurements from the topside.

One possible issue with using an active probe is the potential for interference with device operation. In order to evaluate this possibility, testing was performed by illumination of MOS-FET structures with $\sim 100\text{mW}$ of 1020 nm light in a circle of $\sim 1\text{ mm}$ radius. The resultant optical intensity of $\sim 3\text{ W/cm}^2$ is typical of the illumination used in the a backside Schlieren system.

The test devices were MOS-FETs with an area of $\sim 10\text{ }\mu\text{m}^2$. The IV characteristics of the test devices were measured using a HP Semiconductor Parametric Analyzer. IV curves were obtained with and without illumination present. Typical results are shown in Figure 10. The difference of the two IV curves, Figure 11, shows a small positive current of a few nanoamps. This current is sufficiently small that it is unclear if it is due to the optical input or drift in the measurement instrument. If attributed to the optical input, the current is still several orders of magnitude smaller than the device leakage current. This small amount of current is not expected to produce measurable effects in a digital circuit. Some, highly sensitive, analog circuits could exhibit small offsets effects due to the optical illumination, however.

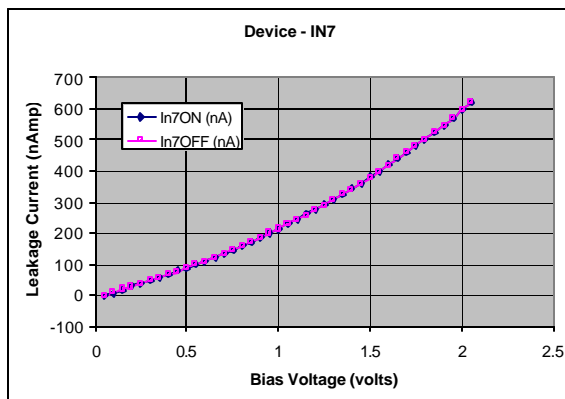


Figure 10 IV characteristics for n-drain to p-well diode with and without optical illumination. Curves are virtually identical.

The results of the early prototype STM were sufficiently good to proceed with commercialization of the instrument. The commercial version of the apparatus has a thermal resolution of $\sim 10\text{ mK}$ and a 10 bit, 1024×1024 image format. A photo of the manufacturing prototype is shown in Figure 12.

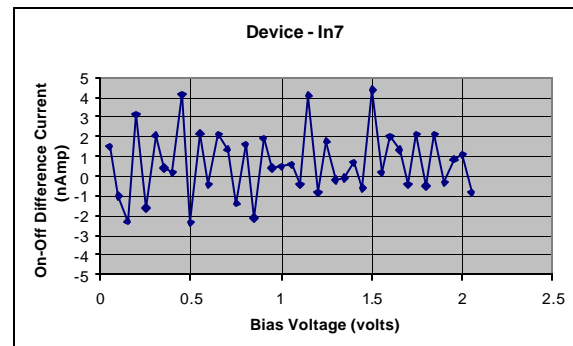


Figure 11 Difference of curves in Figure 10. A slight positive bias is seen.



Figure 12 Manufacturing prototype of STM showing optical head on vertical tower and electronics control box. Computer control system is not shown.

Device Preparation

The quality of device preparation is critical to the success of any failure analysis procedure. In the case of backside imaging, several unique issues occur. For example, heavily doped silicon substrates are highly absorptive at short wavelengths due to bandgap absorption and at long wavelengths due to free carrier absorption. A window in the absorption occurs in the near infrared as shown in Figure 13. Even within that window, the absorption of the silicon substrate can be sufficient to render imaging impossible. Thus, the most highly doped substrates must be thinned to around $200\text{ }\mu\text{m}$ [1].

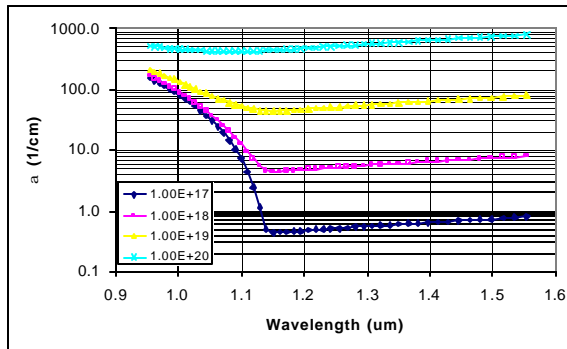


Figure 13 Results of empirical model of absorption in p doped silicon.

Clearly the back surface of the substrate should be polished to an optical quality surface. In addition, the high refractive index of silicon in the near infrared, ~ 3.6 , causes approximately 32% of the light entering the substrate to be reflected back into the detection apparatus. This glint can totally swamp out the image signal in any active imaging system and must be reduced through use of anti-reflection coatings. A single layer quarter-wave coating of a material such as silicon monoxide can reduce this reflection to less than 0.5%. Services and coating machines are readily available for producing these coatings.

Summary and Conclusions

Active, phase-contrast imaging opens the opportunity to re-establish topside thermal mapping techniques to backside failure analysis. Schlieren thermal imaging, a particular form of phase-contrast imaging, has demonstrated thermal sensitivities on the order of 10 mK. Time resolution is limited only by the duration and intensity of the laser source, with nanosecond resolutions being demonstrated.

Future efforts include demonstration of the techniques for topside thermal mapping, application to other material systems, e.g. silicon on insulator, improved imaging resolution and improved thermal sensitivity.

Acknowledgements

Funding for this work derived in part from the US Air Force, Sandia National Laboratories, and the SEMATECH Product Analysis Forum.

References

1. R. A. Falk, "Near IR Absorption in Heavily Doped Silicon – An Empirical Approach" published in this conference.
2. D.T.F. Marple, *J. Appl. Phys.* **35**, 1241 (1964)
3. Y.P. Varshni, *Physica* **34**, 149 (1967)
4. *Properties of Silicon*, INSPEC, 72-78 (1988)
5. K. Bucher, J. Bruns, and H. G. Wagemann, *J. Appl. Phys.* **75**, 1127-32 (1994)
6. L.A. Vasil'ev, *Schlieren Methods*, Israel Prog. Scientific Translations (1971)
7. R.A. Falk, F.J. Zutavern, and M.W. O'Malley, *SPIE* vol. 3322, pp. 243-54 (1997)